Stochastic Method to Predict Effects of Roll Grinding Deviations on Sheet Flatness in Cold Rolling

Feng Zhang[1]
Mem. ASME
Department of Mechanical Engineering,
Erik Jonsson School of Engineering and Computer Science,
The University of Texas at Dallas,
800 W. Campbell Road,
Richardson, TX 75080
e-mail: feng.zhang@utdallas.edu

Arif Malik[2]
Mem. ASME
Department of Mechanical Engineering,
Erik Jonsson School of Engineering and Computer Science,
The University of Texas at Dallas,
800 W. Campbell Road,
Richardson, TX 75080
e-mail: arif.malik@utdallas.edu

Industrial measurements of the diameter profiles of work-rolls used in cold sheet rolling are applied with a stochastic roll-stack model to better understand how residual error from the roll grinding process affects the rolled sheet flatness quality. Roll diameter measurements taken via a noncontact, optical device on new, warm, and worn work-rolls show that the diameter deviations vary along the roll lengths, across roll samples, and at different operational states, suggesting a multidimensional random field problem. Studies are conducted for a 4-high rolling mill with 301 stainless steel sheet to investigate the reliability in achieving target flatness considering the work-roll diameter random field. Also investigated is the sensitivity of the flatness reliability to roll diameter deviations at different locations along the roll lengths and for the three operational states (newly machined, warm, and worn following several passes). The results lead to several key findings. Foremost, it is shown that an assumption of statistical independence among the residual grinding errors at different roll axis locations is improper. Furthermore, it is demonstrated that, for the measured grinding error correlation patterns, the roll diameter deviations external to the roll/sheet contact region play an important role in contributing to flatness defects within the sheet and that these influences vary according to the roll operational state (new, warm, worn). The presented stochastic model and applied measurement data thus provide for a new understanding into how roll grinding performance influences dimensional quality in the sheet rolling process. [DOI: 10.1115/1.4052969]

Keywords: cold rolling, roll grinding error, sheet flatness, stochastic analysis, random field, bulk deformation processes (e.g., extrusion, forging, wire drawing), modeling and simulation, sheet and tube metal forming

Introduction

In the cold rolling of thin-gauge steel, aluminum, copper, and brass sheet or strip, the precision of the diameter profiles machined onto the work-rolls is pivotal to attaining required sheet flatness (or shape) dimensional quality criteria. Regardless of the alloy type, when the nominal sheet thickness is less than about 0.5 mm, mill operators can usually detect increased sensitivity of the sheet's flatness to very minor changes in the work-roll diameter profiles. This is a consequence of the relatively large ratios of roll diameter deviations to the sheet thickness, which can cause significant transverse (width-wise) variations in the longitudinal stress and possible localized buckling [1,2], as well as surface quality defects [3,4]. Even with modern computer numerical control (CNC) equipped roll grinding machines, significant deviations in the work-roll diameter profiles can occur, stemming particularly from the vibrations modes inherent to cutting processes [5]. Figures 1(*a*)–1(*d*), respectively, show a typical 4-high cold rolling mill stand, the depiction of a roll diameter random variables, the measured diameter profiles for a work-roll under three operational states ("new," "warm," and "worn"), and an example of highly localized flatness defects that can be generated by high-fidelity roll diameter deviations. The warm roll diameter profile shown in Fig. 1(*c*) was measured following a single rolling pass, while the worn roll profile was measured after several passes and at room temperature. All measurements were taken with an optical roll profiler having accuracy and repeatability to within 0.5 μm. Figure 1(*c*) shows that the diameter profile deviations include micro-scale "bumps" and "flats" in addition to both broad and regional irregularities over the length of the work-roll. Since the particular work-roll diameter shown is intended to have a perfectly uniform profile when machined, the inspection measurements show that the grinding errors propagate to subsequent states, and they in fact become locally amplified when the roll is heated during rolling by friction and plastic heat dissipation from the sheet; diameter peaks for the warm roll are clearly seen to sharpen, while troughs become deeper. The associated flatness defects generated in the rolled sheet, e.g., Fig. 1(*d*), can be complex and difficult to detect visually without interrupting the rolling process and releasing applied entry and exit tensions. Although such localized flatness defects can be detected using online shape meters (e.g., via stress distribution sensors), they are often difficult to eliminate during rolling through the use of conventional flatness control mechanisms.

This issue is complicated further since the roll diameter deviations are transient in nature due to the time-dependent, thermally induced radial strains as well as the gradual wear of sharp profile features during continued rolling. Despite this, and as noted earlier, studies to predict the detailed effects that micro-scale roll diameter deviations have on the sheet thickness profile and flatness are limited [6]. Linghu et al. [7] and Zhang et al. [2] each provide a comprehensive review of the existing roll-stack modeling efforts where the researchers have adapted industrial measurements of work-roll diameter profiles to predict their influences on the transverse distributions of contact force (or stress), sheet thickness profile, or flatness. The drawback of the prior studies, however, is that they do not account for the randomness that exists in the micro-scale variations of diameter profiles among different work-rolls and

[1]Present address: GE Global Research.
[2]Corresponding author.
Manuscript received July 18, 2021; final manuscript received November 2, 2021; published online December 3, 2021. Assoc. Editor: Yannis Korkolis.

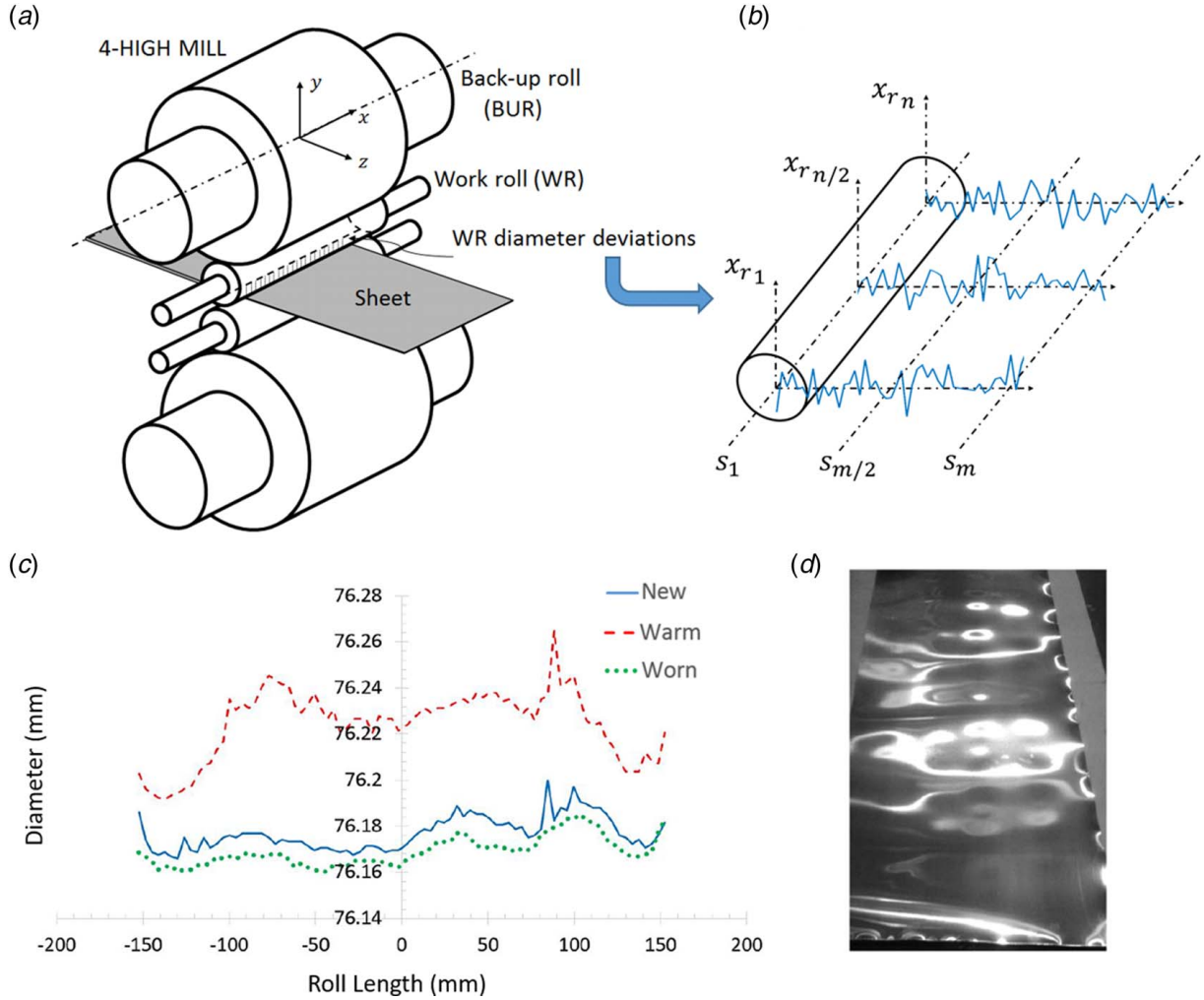

Fig. 1 Cold rolling process considering random roll diameter deviations along the length of the upper work-roll due to residual grinding error: (*a*) schematic of 4-high mill stand; (*b*) depiction of a roll diameter *random field*, characterized by *n* correlated random variables according to the measurement locations across roll samples, *s*; (c) measured work-roll diameter profiles at three operational states that represent the new roll (after grinding), the warm roll after one rolling pass, and the worn roll after cooling to room temperature following several rolling passes. Note: accuracy and repeatability of the noncontact optical measurement device are ±0.5 μm; (*d*) example of high-fidelity sheet flatness defects.

particularly at varying operational states during rolling, such as the new, warm, and worn conditions in Fig. 1(*c*). While transient rolling models can be developed and directly applied to accommodate time-dependent, deterministic (nonrandom) roll profile variations, the work described in this article shows that a stochastic computational mechanics approach involving three-dimensional roll-stack deformations computed together with measured work-roll profiles can provide a very useful approach that also gives important new insights into the effects of work-roll diameter deviations in achieving desired flatness quality criteria.

Previously, the stochastic analysis has been widely applied directly to the grinding process [8]. Newly ground cylinders (rolls) can be subject to grinding errors that vary continuously across the cylinder length and change disproportionately with use over time, as shown in Fig. 1(*c*). In fact, Peklenik was the first to experimentally observe that grinding deviations exhibit randomness over the ground surface and thus discussed the use of spatial correlations to characterize the surface topography [9,10]. Accordingly, the practice of roll grinding can be generally considered a multidimensional, spatially fluctuating random process, which is typically referred to as a *random field* [11]. Although both Gaussian and non-Gaussian random fields have been used to classify the distributions of ground profiles, in reality, the surface represents the synthesis of several complex factors, including roughness, waviness, and form error [12]. Referring again to Figs. 1(*a*) and 1(*b*), consider for the purposes of this study that the top work-roll of the 4-high mill contains residual grinding error (diameter deviation) characterizable as a random field. A set of measurements taken offline indeed reveals that the diameter varies over the roll length position (x), across samples of different rolls (s), and because of the thermal strain and wear during rolling, the residual grinding error also varies with time (t).

As mentioned earlier, such multidimensional spatially fluctuating work-roll diameter profiles render flatness control methods such as rolling bending and roll shifting inefficient or even ineffective because they inherently correct for low- and medium-fidelity flatness defects [2]. In fact, precision nozzle systems for localized differential roll cooling represent the only feasible online control mechanism for attenuating higher-fidelity flatness defects [13]. This is because the defects like those shown in Fig. 1(*d*) are strongly related to the local contact force and reduction relationship, which is a function of the friction coefficient [14] and which, in turn, is affected by the specific spraying nozzle pattern, spray angle, and lubrication mixing device [15]. Therefore, integration of a thermal model into an online control system involving multiple roll cooling headers can enable in situ control of the work-roll diameter profile, with the control fidelity and response time governed by the number of nozzles and the relative rates of heat conduction and convection

along the roll length. Spray header cooling, however, is not possible on some important mill types such as 20-high or 12-high cluster mills in which the entire roll-stack is flooded with lubricant. Notwithstanding the merits of differential roll cooling to help mitigate localized sheet flatness defects, there is still an absence of comprehensive understanding as to how well spray header nozzle systems address the random field variability of the work-roll diameter profiles, and in particular, the quantitative effects that the spatial correlations pose to the likelihood of achieving a desirable sheet thickness reduction profile and associated flatness quality.

Since gaining a fundamental understanding of the effects that roll diameter random fields have on the sheet thickness and flatness is prudent to any subsequent model adaption into a real-time control system (such as spray header cooling), the aim of this article is to introduce a rigorous mathematical method to facilitate this understanding. Introduced is a stochastic simplified-mixed finite element method (SSM-FEM), which integrates the existing simplified-mixed finite element method (SM-FEM) used to predict three-dimensional roll-stack contact mechanics, with a first-order reliability method (FORM) to accommodate the random field contribution.

Note that in the previous work, the conventional (nonstochastic) SM-FEM roll-stack deformation model has shown strong prediction capability compared with industrial measurements of rolled sheet thickness profiles, as well as to large-scale continuum finite element (FE) modeling approaches incorporating high-fidelity roll diameter deviations [1,16]. Moreover, the conventional SM-FEM model exhibits very rapid calculation time, performing static simulations in seconds versus hours required of the large-scale continuum FE model to which it was compared. The convergence studies with the large-scale FE model exhibited trends in displacements toward those of the SM-FEM, thus also underscoring accuracy of the SM-FEM approach. A *stochastic* simplified-mixed finite element method is to be formulated here by incorporating the FORM mathematical technique for the random field into the SM-FEM roll-stack model. The purpose is to understand the influence of roll diameter random fields on the sheet thickness reduction, as well as to be able to infer probabilities as to whether high-fidelity flatness defects will occur and thus to gain new insights into how roll grinding processes might be improved to reduce such probabilities.

FORM constitutes a class of analytical, safety index-based reliability approaches in which both limit-state functions and statistical variances are estimated using first-order Taylor series approximations [17]. FORM has been applied in diverse fields, particularly engineering design, to estimate reliability and to understand how uncertainties influence the resulting reliability. Compared to sampling-based approaches such as Monte Carlo simulation, FORM offers a practical and efficient reliability estimation, particularly when applied with large numbers of correlated random variables, as is the case in this work [18].

In Mathematical Formulation section, mathematical formulation of the SSM-FEM three-dimensional stochastic roll-stack model is presented, together with advantages and disadvantages relative to alternative approaches. Results and Discussion section first illustrates the utility of the proposed SSM-FEM to highlight the importance of considering the work-roll diameter deviations as a random field. Afterward, the SSM-FEM is used to predict the reliability effects of the sheet flatness based on work-roll conditions in the new, warm, and worn operational states. Included in the reliability analysis is an estimate of the probability of achieving a target sheet flatness based on permissible deviation limits to the normalized average thickness reduction. The stochastic analysis directly considers the influence of spatial correlations amongst the work-roll diameter deviations at the numerous measurement locations along the work-roll length.

Mathematical Formulation

The SSM-FEM is described, with the stochastic components discussed first. The FORM is then reviewed, together with a demonstration on how the random field is addressed. The necessary equations for the existing, deterministic SM-FEM are also then briefly introduced [1,6,16,19].

Consideration of the Work-Roll Diameter Deviation as a Random Field. The random field for the work-roll diameter deviation (or error) is denoted $\boldsymbol{e}(\boldsymbol{x_r}, \boldsymbol{s})$, which can be discretized into a finite number of correlated random variables over the roll axis length, $\boldsymbol{x_r} = [x_{r_1}, x_{r_2}, \ldots, x_{r_n}]^T$, and across different work-roll samples, $\boldsymbol{s} = [s_1, s_2, \ldots, s_m]^T$. Based on the measurements taken, Fig. 2 shows the corresponding means, standard deviations, and linear (Pearson) correlation coefficients for the roll diameter deviations along $\boldsymbol{x_r}$. Note that, for brevity, correlation coefficients are shown only at three positions along the roll axis (left, center, and right). These statistics shown in Fig. 2 also capture the three operational states examined for the work-roll, i.e., the new roll state ($\boldsymbol{e}_{new}$) representing residual grinding error, the warm state ($\boldsymbol{e}_{warm}$) indicating diameter deviations after one rolling pass, and the worn state ($\boldsymbol{e}_{worn}$) indicating deviations after several rolling passes (and subsequent cooling to room temperature). Note that in a conventional correlation decay relationship, as the proximity between any two random variables is reduced, the strength of their correlation decreases until the respective random variables are essentially considered to be independent. However, the industrial measurements in Fig. 2 reveal that a "W"-shaped correlation decay relationship exists along $\boldsymbol{x_r}$, possibly due to vibration or fixturing of the work-roll during grinding. Note that the standard deviation profile is also characterized by a "W" shape, but with regional fluctuations as well. In addition, when the roll is warm, thermal expansion amplifies the means in the region where the majority of contact with the rolled sheet occurs. Standard deviations are also increased over much of the roll length, but not uniformly. Interestingly, additional spatial correlation is created in the warm diameter deviation, $\boldsymbol{e}_{warm}$. In the worn work-roll, the wear seems to generally reduce the statistical means along $\boldsymbol{x_r}$, but it also changes the correlations slightly in $\boldsymbol{e}_{worn}$.

To enable the calculation of the sheet flatness reliability, it is first assumed (according to convention) that deviations from the average normalized thickness reduction are directly related to the change in sheet flatness during rolling due to the incompressibility condition of plastic deformation and the negligible expansion of the strip width [20]. Thus, based on Eqs. (1) and (2), a reduction deviation, $\Delta\boldsymbol{r}$, is defined based on normalized thickness reduction, r, minus average normalized thickness reduction, $\bar{r}$.

$$\Delta\boldsymbol{r}(\boldsymbol{x_d}, \boldsymbol{e}(\boldsymbol{x_r}, \boldsymbol{s})) = \boldsymbol{r}(\boldsymbol{x_d}, \boldsymbol{e}(\boldsymbol{x_r}, \boldsymbol{s})) - \bar{\boldsymbol{r}}(\boldsymbol{x_d}, \boldsymbol{e}(\boldsymbol{x_r}, \boldsymbol{s})) \tag{1}$$

where

$$\boldsymbol{r}(\boldsymbol{x_d}, \boldsymbol{e}(\boldsymbol{x_r}, \boldsymbol{s})) = 1 - \boldsymbol{h}(\boldsymbol{x_d}, \boldsymbol{e}(\boldsymbol{x_r}, \boldsymbol{s}))/\boldsymbol{H}(\boldsymbol{x_d}, \boldsymbol{e}(\boldsymbol{x_r}, \boldsymbol{s})) \tag{2}$$

Note that $\boldsymbol{r}$ is obtained from the entry and exit thickness profiles, $\boldsymbol{H}$ and $\boldsymbol{h}$, respectively. The reduction deviation, $\Delta\boldsymbol{r}$, is a dimensionless vector of thickness reduction deviations used here to quantitatively estimate proportionate (scaled) local flatness changes across the sheet width. For a given entry sheet thickness profile, the exit thickness profile, $\boldsymbol{h}$, is calculated deterministically using the conventional SM-FEM, introduced later in this section.

In the aforementioned equations, note that $\boldsymbol{x_d} = [x_{d_1}, x_{d_2}, \ldots, x_{d_p}]$ refers to the discrete locations along the roll length for the deterministic roll-stack contact mechanics using SM-FEM, and thus, $\boldsymbol{x_d}$ is distinct from $\boldsymbol{x_r}$ used for the random field "element" discretization. Hence, the stochastic FEM for a continuum structure includes two "mesh" types: (1) a regular element mesh, indexed "i" for the SM-FEM; and (2) a random field element mesh, indexed "*i*" for stochastic analysis. Because the random field mesh is generally not as dense as that needed for the roll-stack model, the middle point method and the spatial averaging method that Vanmarcke and Grigoriu developed [21], as well as the Karhunen–Loeve expansion method and Newmann expansion that Shinozuka and Deodatis developed [22], can provide interpolation to give a continuous

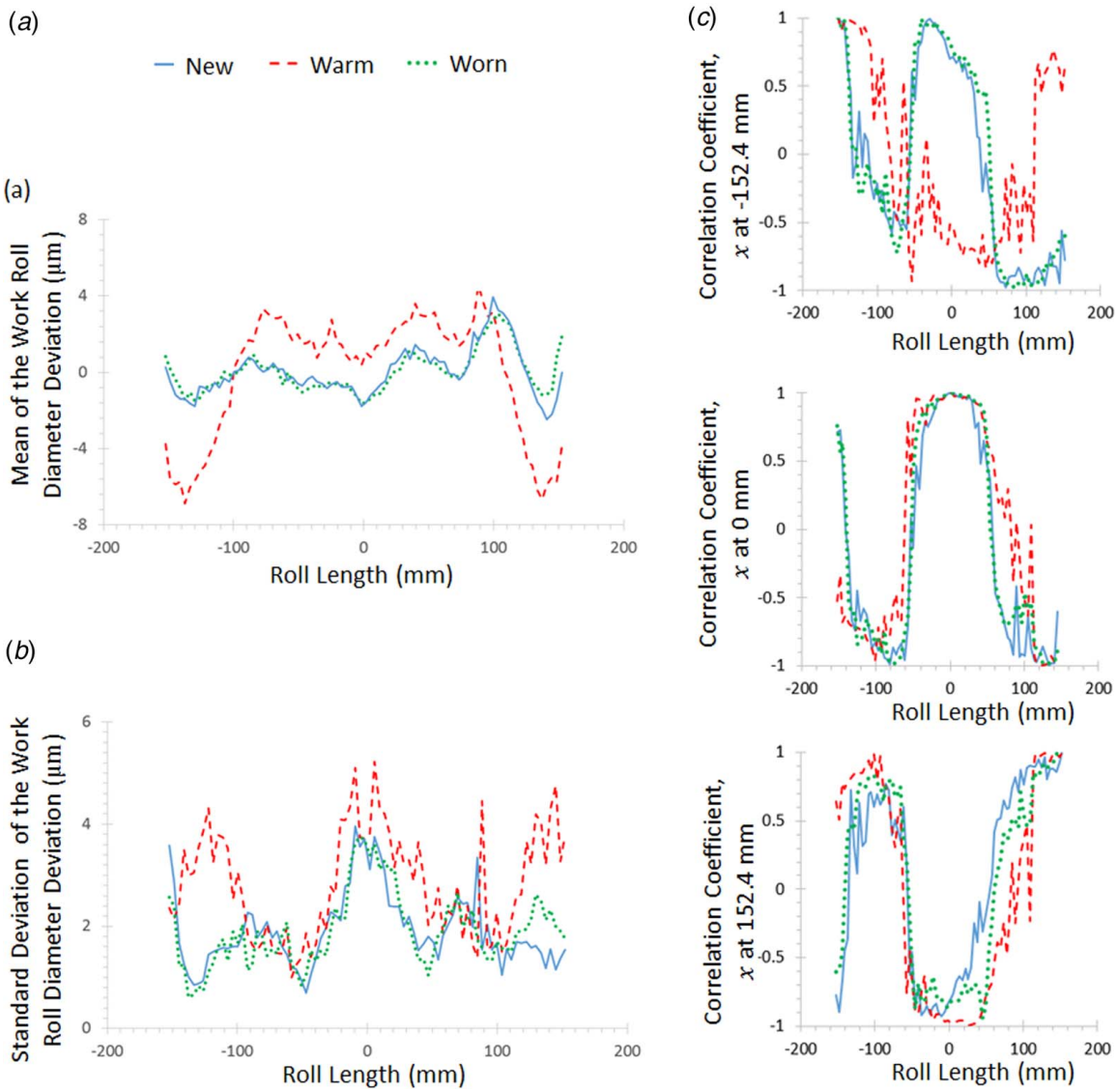

Fig. 2 Work-roll diameter deviation statistics for 82 measurement locations at equal intervals along roll length with 246 total samples. (*a*) Mean, (*b*) standard deviation, and (c) correlation coefficients computed at three roll axis locations: left end of roll (top right image), midpoint of roll (center right image), and right end of roll (bottom right image). Note: accuracy and repeatability of the noncontact optical measurement device is $\pm 0.5\,\mu$m.

random field for use within the discrete roll-stack model mesh. In this article, the random field mesh fidelity stems directly from the measurement data; since Fig. 2 includes 82 points (246 total samples) measured at 12.7 mm intervals along the 304.8 mm length work-roll, this discrete set establishes the random field mesh. For the roll-stack model mesh described later, its density is based on displacement convergence using foundation elements coupled to Timoshenko beam elements having 5 Gauss points (integrating ninth order polynomials exactly) [23]. The SSM-FEM method created in this study applies linear interpolation between the random field mesh and the SM-FEM roll-stack mesh.

Given the definition of thickness reduction deviation, $\Delta \boldsymbol{r}$, from Eq. (1), a sheet flatness failure criterion can be established to define a limit-state function, $g(\boldsymbol{e})$. Here, $g(\boldsymbol{e})$ is based on whether the maximum absolute value of the reduction deviation exceeds a target threshold, Δr_t, at any location in $\boldsymbol{x_d}$, as given in Eq. (3). The absolute value accounts for both positive and negative longitudinal plastic strains of the sheet (i.e., relatively looser and tighter local flatness changes across the sheet's width).

$$g(\boldsymbol{e}) = \Delta r_t - \max\left[|\Delta r(\boldsymbol{x_d}, \boldsymbol{e})|\right] \tag{3}$$

As is the convention with FORM, $g(\boldsymbol{e}) = 0$ represents the failure threshold between safe regions in the probability space governed by $g(\boldsymbol{e}) > 0$ and failure regions for which $g(\boldsymbol{e}) \leq 0$. Given the associated joint probability density function (PDF), $f_{\boldsymbol{e}}(\boldsymbol{e})$, for the work-roll diameter deviations, integration of $f_{\boldsymbol{e}}(\boldsymbol{e})$ over the safe probability region, $g(\boldsymbol{e}) > 0$, yields the analytical reliability, P_R, which represents the probability of not realizing any sheet defects:

$$P_R = \int_{g(\boldsymbol{e})=0}^{g(\boldsymbol{e})>0} f_{\boldsymbol{e}}(\boldsymbol{e}) d\boldsymbol{e} \tag{4}$$

In general, unless the joint PDF, $f_{\boldsymbol{e}}(\boldsymbol{e})$, is available in a closed form and can be integrated, reliability estimations are instead made either through sampling-based statistical inferences (i.e., Monte Carlo simulation) or through analytical safety-index type approximations. Due to the relatively high number of 82 correlated random variables in $\boldsymbol{e}$, a FORM safety-index reliability approach is adopted for the stochastic analysis, as outlined next.

First-Order Reliability Method. In FORM, the calculated reliability, P_R, is given in Eq. (5), where Φ is the standard,

normal, cumulative distribution function. P_R is exact only for linear limit-state functions, g, with statistically independent, normally distributed random variables. In all other cases, FORM provides an approximation according to the nonlinearity of g and the distribution types for the random variables. As shown in Eq. (5), however, a reliability estimate with correlated nonnormal random variables can be made through transformation to equivalent, normally distributed variables.

$$P_R = \Phi(\beta) \tag{5}$$

In Eq. (5), the term β, which is denoted the reliability index, is the shortest distance between the origin of the *reduced* independent random variables, $\boldsymbol{v}$, and the limit-state surface. β is defined as the ratio of the mean of limit-state function g to the first-order estimate of the standard deviation of g [24], i.e.,

$$\beta = \mu_{g(\boldsymbol{v})}/\sigma_{g(\boldsymbol{v})} \tag{6}$$

In Eq. (6), $\boldsymbol{v}$ is the vector of independent random variables in the reduced domain. Equation (7) shows the transformation from the original, correlated random variables, $\boldsymbol{e}$, into $\boldsymbol{v}$:

$$\boldsymbol{e} = \boldsymbol{STv} + \boldsymbol{M} \tag{7}$$

where $\boldsymbol{S}$ is the diagonal matrix of equivalent normal standard deviations, $\boldsymbol{\sigma}_{\boldsymbol{e}}^N$, and $\boldsymbol{M}$ is the vector of equivalent normal means, $\boldsymbol{\mu}_{\boldsymbol{e}}^N$, as shown in Eqs. (8) and (9):

$$\boldsymbol{S} = \begin{bmatrix} \sigma_{e_1}^N & \cdots & 0 \\ \vdots & \ddots & \vdots \\ 0 & \cdots & \sigma_{e_n}^N \end{bmatrix} \tag{8}$$

$$\boldsymbol{M} = [\mu_{e_1}^N,\ \mu_{e_2}^N, \ldots, \mu_{e_n}^N]^T \tag{9}$$

Since it is unlikely that $\boldsymbol{e}$ includes all normal variables, equivalent normal parameters, $\boldsymbol{\sigma}_{\boldsymbol{e}}^N$ and $\boldsymbol{\mu}_{\boldsymbol{e}}^N$, need be defined by either a two-parameter [25] or three-parameter [26,27] equivalent normal approach. The transformation matrix $\boldsymbol{T}$ in Eq. (7) includes normalized eigenvectors of the correlation coefficient matrix, $\boldsymbol{R}$, in Eq. (10), which consists of the correlation coefficients, $\rho_{e_{xr_i}, e_{xr_j}}$, between original random variables $\boldsymbol{e}(x_{r_i}, \boldsymbol{s})$ and $\boldsymbol{e}(x_{r_j}, \boldsymbol{s})$, and where $\rho_{e_{xr_i}, e_{xr_j}} = 1$ on the main diagonal of $\boldsymbol{R}$ for $i = j$.

$$\boldsymbol{R} = \begin{bmatrix} \rho_{e_{xr_1}, e_{xr_1}} & \cdots & \rho_{e_{xr_1}, e_{xr_n}} \\ \vdots & \ddots & \vdots \\ \rho_{e_{xr_n}, e_{xr_2}} & \cdots & \rho_{e_{xr_n}, e_{xr_n}} \end{bmatrix} \tag{10}$$

The square roots of the corresponding eigenvalues of $\boldsymbol{R}$ give the equivalent normal standard deviations, $\boldsymbol{\sigma}_{\boldsymbol{v}}^N$, of the reduced, uncorrelated variables $\boldsymbol{v}$. Note that correlation coefficient values in $\boldsymbol{R}$ depend on the estimation procedure and available data; the case can occur in which the resulting matrix is not positive semi-definite. In this scenario, it might be desirable to find the "closest" positive semi-definite matrix relative to some error measure. Note, however, that even if a nonpositive semi-definite $\boldsymbol{R}$ leads to several negative eigenvalues that are very close to zero, the square roots of these negative eigenvalues are generally too small to significantly influence the reliability.

For nonlinear g, an optimization problem arises in the aforementioned procedure such that reliability index β is minimized subject to the threshold constraint $g(\boldsymbol{e}^*) = 0$. The gradient-based iterative optimization procedure using Eqs. (11)–(14) is typically used. In Eq. (11), the "*" represents the iterated variables. Also, note that $\boldsymbol{\sigma}_{\boldsymbol{v}}^N$ and $\boldsymbol{T}$ remain consistent because they depend on the measured correlations of $\boldsymbol{R}$.

$$\boldsymbol{v}^* = -\boldsymbol{\alpha}^* \beta^* \boldsymbol{\sigma}_{\boldsymbol{v}}^N \tag{11}$$

The vector $\boldsymbol{\alpha} = [\alpha_1, \alpha_2, \ldots, \alpha_n]^T$, defined by Eq. (12), contains the n direction cosines of β, and thus constitutes components of the normalized gradient vector of the limit-state function g:

$$\alpha_i = \left(\frac{\partial g}{\partial v_i}\sigma_{v_i}^N\right) \Bigg/ \sqrt{\sum_{i=1}^{n}\left(\frac{\partial g}{\partial v_i}\sigma_{v_i}^N\right)^2} \tag{12}$$

Because $\boldsymbol{v}$ has no physical meaning relative to limit-state function g and because the $\dfrac{\partial g}{\partial v_i}$ similarly do not represent physical values, a chain rule transformation is required to transform $\boldsymbol{v}$ back to the original, correlated random variables, $\boldsymbol{e}$:

$$\frac{\partial g}{\partial \boldsymbol{v}} = \frac{\partial g}{\partial \boldsymbol{e}}\frac{\partial \boldsymbol{e}}{\partial \boldsymbol{v}} \tag{13}$$

The chain rule transformation mentioned earlier is analogous to Der Kiureghian and Ke transformation by Jacobian matrix [18].

Substitution of Eqs. (7) and (13) into Eq. (12) gives:

$$\alpha_i = \left(\frac{\partial g}{\partial e_i}\ \mathrm{diag}(\boldsymbol{ST})\sigma_{v_i}^N\right) \Bigg/ \sqrt{\sum_{i=1}^{n}\left(\frac{\partial g}{\partial e_i}\mathrm{diag}(\boldsymbol{ST})\sigma_{v_i}^N\right)^2} \tag{14}$$

The main effort in the FORM implementation here is to iteratively find the minimum reliability index, β^*, subject to the constraint $g(\boldsymbol{e}^*) = 0$. Once converged, the most probable points (MPP) of failure, $\boldsymbol{v}_{MPP}$ and $\boldsymbol{e}_{MPP}$, can be found. One of the most significant features of FORM is its ability to give the sensitivity of the computed reliability to each variable in the random field. The unit sensitivity index vector, $\boldsymbol{\gamma}$, can be calculated to express the contribution of each correlated random variable in $\boldsymbol{e}$ to the total reliability:

$$\boldsymbol{\gamma} = \frac{\boldsymbol{SB}'\boldsymbol{\alpha}_{MPP}}{|\boldsymbol{SB}'\boldsymbol{\alpha}_{MPP}|} \tag{15}$$

where

$$\boldsymbol{B} = (\boldsymbol{ST})^{-1} \tag{16}$$

If the work-roll diameter deviations in $\boldsymbol{e}$ happened to be statistically independent, then $\boldsymbol{SB}'$ would become an identity matrix and $\boldsymbol{\gamma}$ would be the same as the vector $\boldsymbol{\alpha}$ from Eq. (14).

Figure 3 is a flowchart summarizing the iterative FORM algorithm used in the SSM-FEM here, in conjunction with the measured work-roll diameter deviations, $\boldsymbol{e}$. To more easily address the computational challenges associated with convergence of the solution, and nonlinearity in the limit-state function, g, two separated convergence loops are implemented, respectively, for $\boldsymbol{\alpha}$ and β.

Simplified-Mixed Finite Element Method to Compute 3D Roll-Stack Contact Mechanics. Unlike for a conventional, large degree-of-freedom, continuum FE roll-stack model, the highly efficient SM-FEM [1] uses Timoshenko beam element stiffness matrices, $\boldsymbol{K}_T$, to accommodate bending and shear deformations, which are coupled to continuous Winker foundation elements, $\boldsymbol{K}_F$, that capture Hertzian contact and elastic-plastic deformation of the rolled sheet. Foundation stiffness $\boldsymbol{K}_F$ is derived using classic analytical solutions for the cylinder/plate contact interferences. The global stiffness matrix, $\boldsymbol{K}_G$, represents a superposition of the stiffnesses for bending, shear, and flattening of the rolls, as well as for linearized elastic-plastic sheet deformation at the nominal rolling pass operating condition:

$$\boldsymbol{K}_G = \boldsymbol{K}_T + \boldsymbol{K}_F \tag{17}$$

For an element i between bodies 1 and 2 (i.e., roll–roll or roll–sheet), respectively, the coupled global stiffness $\boldsymbol{K}_G^{1,2,\mathrm{i}}$ has a size 24 by 24 when all six translational and rotational degrees-of-freedom are retained in each of the four nodes (see two Timoshenko beam elements with intervening foundation in

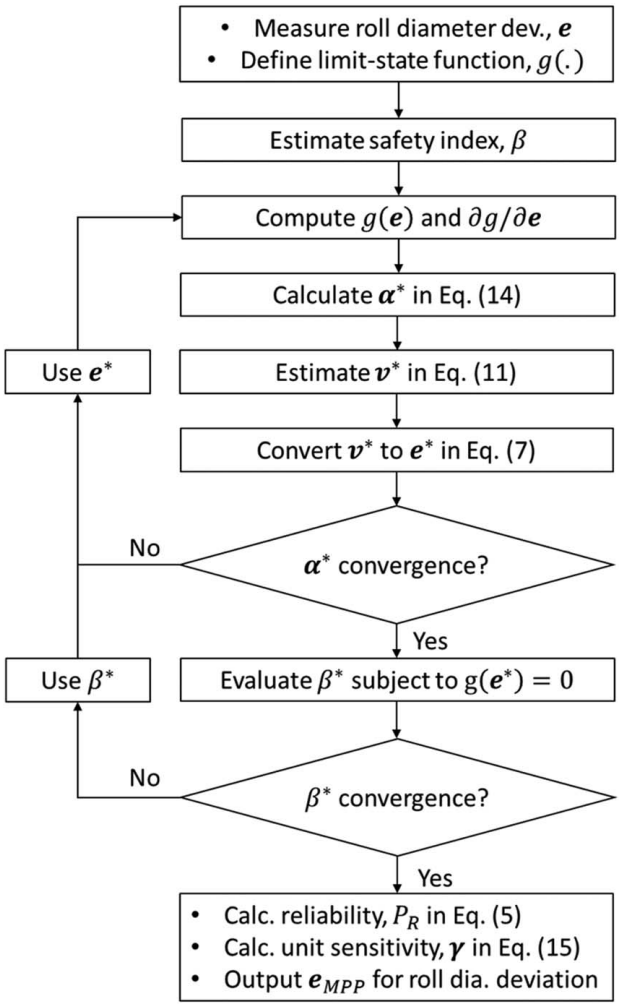

Fig. 3 Flowchart of the SSM-FEM

Fig. 4). $\boldsymbol{K}_F$ is a variable due to its functional dependence on the contact interference, I, which is based on the Hertz contact theory [16] and the linearized elastic-plastic sheet behavior (i.e., unit rolling force versus thickness reduction) at the nominal rolling pass operating condition:

$$\boldsymbol{K}_G^{1,2,\mathrm{i}} = \begin{bmatrix} \int_0^{l_i} k_{feq}(x)\boldsymbol{N}_{11}dx & -\int_0^{l_i} k_{feq}(x)\boldsymbol{N}_{12}dx \\ -\int_0^{l_i} k_{feq}(x)\boldsymbol{N}_{21}dx & \int_0^{l_i} k_{feq}(x)\boldsymbol{N}_{22}dx \end{bmatrix} + \begin{bmatrix} \boldsymbol{K}_T^{1,\mathrm{i}} & [0] \\ [0] & \boldsymbol{K}_T^{2,\mathrm{i}} \end{bmatrix} \tag{18}$$

In Eq. (18), l_i is the ith element length. For the two bodies, $\boldsymbol{N}_{pq}$ (for p, $q \in [1, 2]$) represents the full shape function representing both horizontal and vertical displacements for conventional Timoshenko beams [28]. Full representations of matrices $\mathbf{K}_T$ and $\mathbf{K}_F$ are provided in Ref. [29].

The equivalent foundation modulus, k_{feq}, in Eq. (18) is a series combination of the bulk contact stiffness of body 1, namely k_{f_1}, and the bulk contact stiffness of body 2, namely k_{f_2}, over the arc of contact between bodies 1 and 2 (see Fig. 4, where body 1 is the sheet and body 2 is the work-roll):

$$k_{feq}(x)^{-1} = k_{f_1}(x)^{-1} + k_{f_2}(x)^{-1} \tag{19}$$

For bulk elastic contact stiffness of rolls, e.g., k_{f_2}, the SM-FEM approach can adopt, for example, a classic Hertz or modified (e.g., Ref. [30]) plane–strain analytical relation (for both cylinder-to-cylinder and cylinder-to-plate contact). The equivalent foundation modulus for the rolled sheet, k_{f_1}, can be identified from the secant or tangent in the functional relationship between unit rolling force and sheet reduction at the anticipated operating point [20]. The "mixed" contribution to the stiffness in SM-FEM is thus based on classic analytical solutions for contact interference. Interference is computed from the beam/plate neutral axis displacements with adjustment for bulk surface profile variations such as roll crowning, which directly affects the contact force distribution. The compatibility approach is used to formulate the interference, I_{12}, between the adjacent bodies 1 and 2 (see Fig. 4) based on the distance between their respective axes, d_{12}, as well as their diameters D, and their profile errors e (from the work-roll residual grinding error in the case here). Hence:

$$I_{12} = H/2 + D_2/2 - d_{12} + e \tag{20}$$

$$d_{12} = (y_{2c} - v_2) - (y_{1c} - v_1) \tag{21}$$

where y_{1c} and y_{2c} are to initial vertical axes coordinates, and v_1, v_2 are the vertical displacements of bodies 1 and 2, respectively. If $I_{12} > 0$, the two bodies are in contact; otherwise, contact is lost. The unit contact force and exit strip thickness then are defined as follows:

$$f = k_{eq}\, I \tag{22}$$

$$h/2 = H/2 - I_{12}\, k_{feq}/k_{f_1} \tag{23}$$

A modified Newton–Raphson method is used here to iteratively solve the above nonlinear roll-stack contact problem [19]. Equation (24) represents the corresponding nonlinear system, where the global stiffness matrix, $\boldsymbol{K}_G$, and the global load vector, $\boldsymbol{f}$, are explicitly stated as functions of the nodal displacement vector, $\boldsymbol{u}$, which contains all six translational and rotational degrees-of-freedom at each node.

$$\boldsymbol{K}_G(\boldsymbol{u})\, \boldsymbol{u} = \boldsymbol{f}(\boldsymbol{u}) \tag{24}$$

Results and Discussion

In this section, the first case study represents the deterministic (nonstochastic) analysis comparison between a perfectly ground (smooth) work-roll and a work-roll having diameter deviation profiles represented by the mean values of the residual grinding error (i.e., mean "new" roll profile shown in Fig. 2(*a*)). This deterministic analysis not only illustrates the effect from work-roll diameter deviation but also constitutes the first calculation step in the stochastic analysis. The second case study demonstrates the importance of considering the residual grinding error as a random field (of correlated random variables) rather than simply as a vector of discretely spaced independent random variables. In the third and final case study, the SSM-FEM is applied to compare reliability outcomes using the warm and worn work-roll diameter deviation random fields.

Table 1 provides information for the 4-high mill stand and 301 stainless steel sheet with 0.236 mm entry gauge that are used in the analyses. The target threshold for reduction deviation, Δr_t, is ± 0.0005 at any point across the sheet width based on an arbitrary but typical industrial expectation in avoiding excessive sheet flatness defects. In the case studies that follow, note that only the top work-roll is considered to include the diameter profile deviations; the remaining rolls are assumed to have perfectly smooth diameter profiles, but a positive work-roll bending force of 52 kN/side is applied to avoid significant wavy edge flatness defects arising from the typical, natural mill stand deformation.

Case Study 1: Deterministic Analysis. Figure 5(*a*) shows a desired work-roll diameter profile curve, labeled "without $\bar{\boldsymbol{e}}_{new}$," which is intended to be perfectly smooth, parabolic, and symmetric

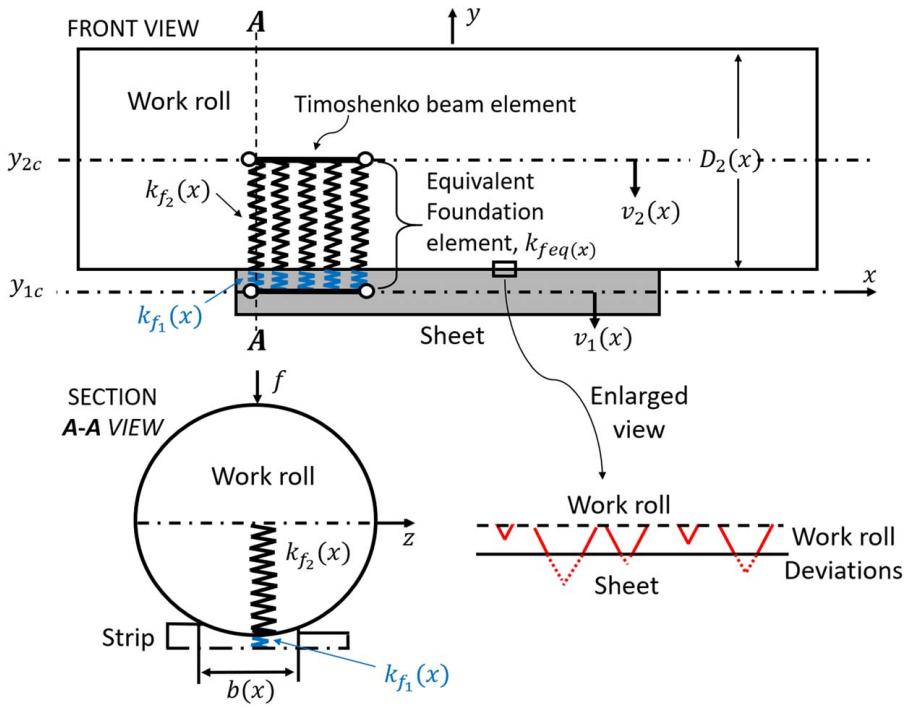

Fig. 4 Depiction of SM-FEM modeling approach for work-roll/sheet contact deformation: front view (top), section view (bottom left), and enlarged view of the contact interface between the sheet and work-roll, showing diameter deviations (bottom right)

Table 1 Dimensions and property information for 4-high mill and 301 stainless steel sheet

Work-roll diameter (mm)	50.8
Back-up roll diameter (mm)	304.8
Roll length (mm)	304.8
Roll elastic modulus (GPa)	200.07
Top back-up roll screw down (mm)	0.381
Sheet entry thickness (mm)	0.236
Sheet entry crown (μm)	0.235
Sheet width (mm)	152.4
Sheet (strip) modulus (GPa)	1170
Roll and sheet Poisson ratio	0.28
Work-roll bending force (kN/side)	52

about the roll axis midpoint. For this desired profile, the difference in diameter between the roll center and each edge (i.e., roll crown) is 0.0813 mm. In contrast, the curve "with $\bar{e}_{new}$" in Fig. 5(*a*) represents the mean of the actual, measured work-roll diameter deviations superimposed onto the same roll (measurement error, although not indicated, is ± 0.5 μm).

The application of the profiles with and without residual grinding error from Fig. 5(*a*) together with the simplified-mixed finite element roll-stack model of the 4-high mill and sheet parameters in Table 1 results in the two respective reduction deviation profiles, $\Delta \boldsymbol{r}$, as shown in Fig. 5(*b*). Note that in both simulations, the entry thickness, H, is assumed to be smooth, symmetric, and parabolic thickness with center-to-edge thickness difference (i.e., entry crown) of 0.235 μm. Figure 5(*b*) also shows reduction deviation threshold lines corresponding to $\pm \Delta r_t$ for both excessively "loose" and "tight" sheet flatness tolerances relative to the average sheet reduction, $\bar{r}$. Without considering the mean grinding error, $\bar{e}_{new}$, the reduction deviation in Fig. 5(*b*) remains symmetric, ranges from -0.000265 to 0.00049, and therefore satisfies the

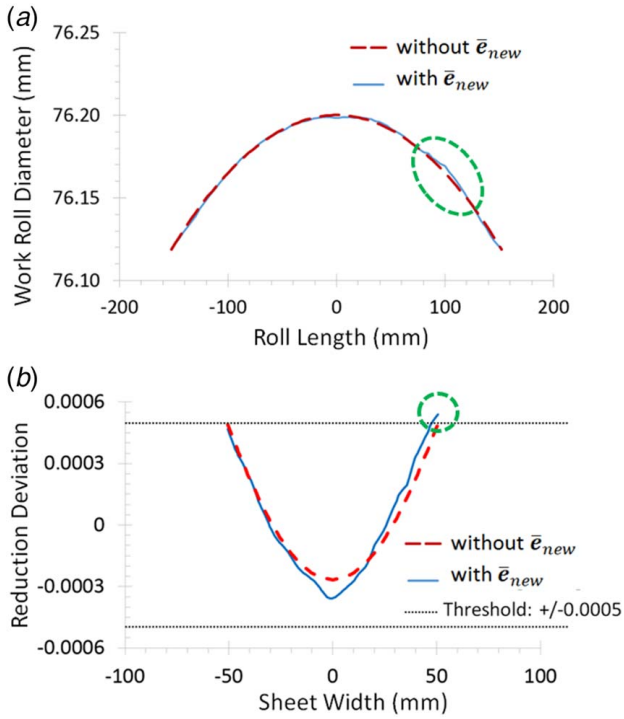

Fig. 5 Comparisons with and without considering the mean work-roll diameter deviations due to residual grinding process error: (*a*) ideal (intended) parabolic work-roll diameter profile, and mean measured work-roll diameter profile with grinding error and (*b*) calculated reduction deviation for rolled sheet (using described roll-stack model), indicating violation of threshold tolerance at right edge of sheet (+50.8 mm) when considering mean roll grinding error

tolerance criterion, $\pm\Delta r_t$. However, upon considering the mean grinding error, $\bar{e}_{new}$, the exit thickness adopts a more "wedge"-shaped profile (differential edge reduction), and the reduction deviation ranges from −0.000359 to 0.000539, which exceeds $+\Delta r_t$. In this particular case, a one-sided wavy edge condition would result since the violated Δr value is positive, and the excessive reduction would correspond to excessive sheet elongation in the rolling direction at the same rightmost edge of the sheet. It worth noting that even though edge trimming is common in sheet rolling, this would normally be accounted for in the target threshold, $\pm\Delta r_t$. This first case study to compare effects of the mean measured work-roll profile with the desired roll profiles serves as a reminder of the risk in sheet flatness predictions that do not take into consideration even the expected (mean) values of work-roll diameter deviations.

Case Study 2: Independent Random Variables Versus Random Field. Although significant progress has been made toward the improvement of roll grinding process, particularly with the advent of CNC, much of the development and most of the applications assume that the residual grinding errors at different locations along the roll length are statistically independent, even if they are considered to possess similar distribution functions and variances. This assumption is shown to be insufficient based on the results discussed next for the same mill and sheet.

Implementation of the described SSM-FEM using the measured work-roll data with the FORM reliability calculation procedure in Fig. 3 leads to the results provided in Table 2. The calculated reliabilities, P_R, presented in Table 2 reflect the probabilities that flatness defects do *not* occur, based on the probability of reduction deviations in the rolled sheet profile being within the target threshold, $\pm\Delta r_t$. Rows 2 and 3 in Table 2 present the following results: (1) a "new" work-roll with the assumption that roll diameters at the 82 measurement locations along the roll length constitute independent random variables ($\boldsymbol{e}_{new_i}$); and (2) a "new" work-roll with statistical information derived from the measurements, wherein roll diameters at the 82 points constitute a correlated random field ($\boldsymbol{e}_{new_c}$). The latter result indicates that the actual correlated residual grinding error gives 38.46% reliability, which is greater than the 35.14% reliability calculated for the independent grinding error assumption. Hence, without considering the correlation, reliability is underestimated. Although the reliability statistic can give guidance regarding the probability of success or failure according to the limit-state function definition, this value alone lacks insight and meaning as to the physical influences underlying both the independent random variable assumption and the random field.

To better understand the physical differences relating to the work-roll profiles, important additional information is shown in Fig. 6(*a*). This figure shows two key aspects in the reliability analysis: (1) the MPP of failure for the work-roll diameter deviation vector, $\boldsymbol{e}_{MPP}$, and (2) the unit sensitivity, $\boldsymbol{\gamma}$, of the reliability to each random variable. In the reliability analysis, the MPP refers to the random variable values most likely leading to the design threshold surface between the safe and failure regions, i.e., probable values of $\boldsymbol{e}$, leading to the limit-state condition $g(\boldsymbol{e}) = 0$ in Eq. (3); in this case, the values and locations of work-roll diameter deviations

Table 2 Summary of the SSM-FEM reliability results for case studies 2 and 3

Work-roll diameter deviation case	No. iterations	Reliability index, β	Reliability, P_R
No deviation $\boldsymbol{e}$	–	–	100% (no failure)
$\boldsymbol{e}_{new_i}$	6	−0.3816	35.14%
$\boldsymbol{e}_{new_c}$	4	−0.2933	38.45%
$\boldsymbol{e}_{warm}$	5	−0.4342	33.21%
$\boldsymbol{e}_{worn}$	4	−0.3230	37.34%

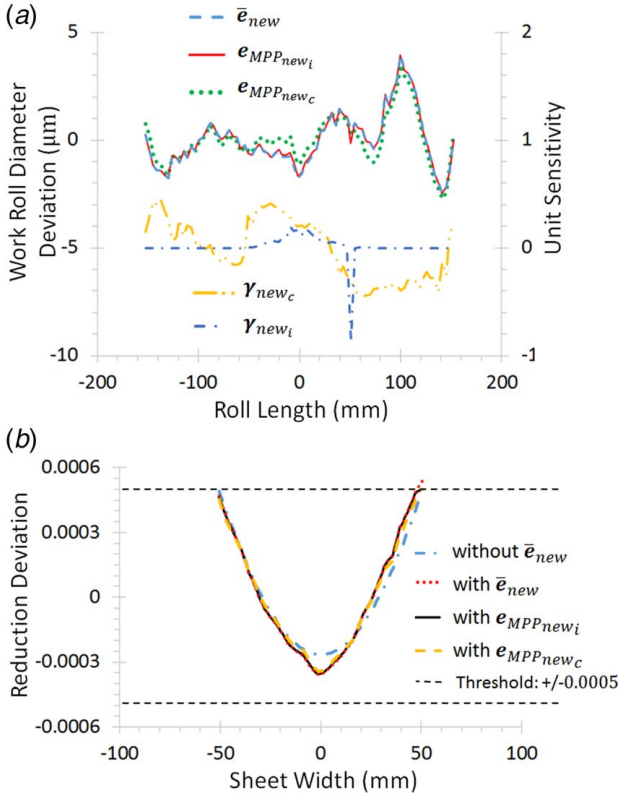

Fig. 6 Comparison of results for "new" roll considering the assumption of independent random variables versus random field (correlated variables) based on measured work-roll diameter deviations: (*a*) mean measured diameter deviation for the new roll ($\bar{e}_{new}$), most probable point (MPP) of failure values on the new roll assuming both independent random variables ($e_{MPP_{new_i}}$) and correlated random variables ($e_{MPP_{new_c}}$), and unit sensitivity (right axis) of the reliability to each random variable on the new roll based on independent variables (γ_{new_i}) and correlated variables (γ_{new_c}) and (*b*) corresponding sheet reduction deviation profiles for mean measured diameter deviation, as well as independent and correlated MPP diameter deviations values on new roll

most likely lead to sheet flatness defects. The sensitivity vector, $\boldsymbol{\gamma}$, from Eq. (15) and also shown in Fig. 6(*a*) (right plot axis) give insights into which random variables affect the reliability most. Both the MPP values and the sensitivity values for the independent random variable assumption and the actual random field (correlated variables) case for the "new" work-roll are shown in Fig. 6. Recall from the previous section's case study that the deterministic analysis indicated that the mean work-roll diameter deviations, $\bar{\boldsymbol{e}}_{new}$, led to unsatisfactory sheet flatness according to the computed reduction deviation, Δr. There exists, however, a design "direction" between mean values, $\bar{\boldsymbol{e}}$, and most probable point of failure values, $\boldsymbol{e}_{MPP}$, that would move the spatially distributed roll diameter deviations from failure toward success (safety). This design direction is contained within $\boldsymbol{\alpha}$, from Eq. (14), which contributes to the calculation of the unit sensitivity, $\boldsymbol{\gamma}$, in Eq. (16). Because from Fig. 5(*b*) the $\bar{\boldsymbol{e}}_{new}$ led to failure of the sheet edge flatness at +50.8 mm along the work-roll length, the independent random variable assumption, $\boldsymbol{e}_{new_i}$, motivates the SSM-FEM model to indicate a required roll diameter change only *locally*, i.e., near the +50.8 mm location on the MPP curve, $\boldsymbol{e}_{MPP_{new_i}}$. Therefore, Fig. 6(*a*) shows that the remedy with the independent assumption is to change the positive work-roll diameter deviation in $\bar{\boldsymbol{e}}_{new}$ to a negative deviation in $\boldsymbol{e}_{MPP_{new_i}}$. Accordingly, a strong, isolated negative sensitivity in $\boldsymbol{\gamma}_{new_i}$ is indicated around +50.8 mm to adjust the sheet reduction deviation at this point so that it just satisfies the target threshold (see Fig. 6(*b*)

also, which shows the corresponding MPP sheet reduction deviation values). Although these changes between $\bar{e}_{new}$ and $e_{MPP_{new_i}}$ are difficult to visualize and interpret, the sensitivity in Fig. 6(*a*) clearly reveals the effects; in particular, for the independent assumption on the new roll, e_{new_i}, the noncontact region between the work-roll and the sheet has zero sensitivity to the reliability since γ_{new_i} is zero outside the strip edges at ±50.8 mm. In contrast to the independent assumption, however, the random field characterization of grinding error on the new work-roll, e_{new_c}, shows that both the MPP and the unit sensitivity are strongly influenced by the correlation. Indeed, although $e_{MPP_{new_i}}$ and $e_{MPP_{new_c}}$ in Fig. 6(*a*) exhibit the same trend in negatively adjusting (decreasing) work-roll diameter deviations around the +50.8 mm location, note that the MPP for the correlated (random field) case, $e_{MPP_{new_c}}$, reduces the *overall* work-roll diameter deviation rather than simply fixing a spatially isolated problematic value, as is the case with $e_{MPP_{new_i}}$ in Fig. 6(*a*). Interestingly, the random field's unit sensitivity γ_{new_i} in Fig. 6(*a*) reveals that significant areas of the noncontact region, as well as locations 25.4 mm from either side of the edge, also affect the sheet's *localized* flatness change at +50.8 mm. This may seem nonsensical since residual regrinding error in the sheet/roll noncontact region never acts directly on the sheet, but because of the correlation present in the grinding process and because of the 3D nature of the roll-stack contact mechanics, both the roll profiles and the sheet thickness reduction at all locations are in fact coupled. Indeed, as evidenced in the "W" shape of the correlation decay relationship shown earlier in Fig. 2(*c*), the work-roll diameter deviation e at the roll axis midpoint (i.e., $x = 0$ mm) has a strong negative correlation with the diameter near both the left and right ends of the work-roll. However, at the end of the left end, the correlation dramatically increases to a strong positive one. Because the work-roll grinding operation in the machine shop takes place in an axial progression along the roll (e.g., from negative to positive positions along the roll length), the initial residual grinding error at $x = -152.4$ mm (noncontact region between roll and sheet) can in fact determine the residual grinding error in the contact region. The strip local flatness change is thus indirectly affected by the residual grinding error over the noncontact region. An important result here in the stochastic analysis is that the assumptions of independent residual grinding errors is flawed because of *random field* influences on the reliability, MPP, and unit sensitivity. Without considering the correlation, the reliability and unit sensitivity are underestimated, and the MPP only targets the obvious abnormal grinding error locations. The most important insight is that the random field provides an understanding of the connection between the grinding process and rolling process and that the grinding precision cannot be relaxed at regions even where the work-roll does not contact the sheet.

Case Study 3: Stochastic Analysis on Warm and Worn Work-Rolls. Thermal expansion was seen earlier in Fig. 1(*c*) to amplify the residual grinding error although the error is generally more difficult to detect after the roll has been used and is cooled because the diameter deviations are modified by the wear. Since work-roll diameter deviations change with the operational state during rolling (e.g., warm versus worn), the SSM-FEM is applied in this section to analyze the reliability with work-rolls in the warm and worn conditions. Table 2 lists 33.21% reliability for warm roll diameter deviations, e_{warm}, versus a greater 37.34% reliability for the worn deviations, e_{worn}. As a result, sheet flatness

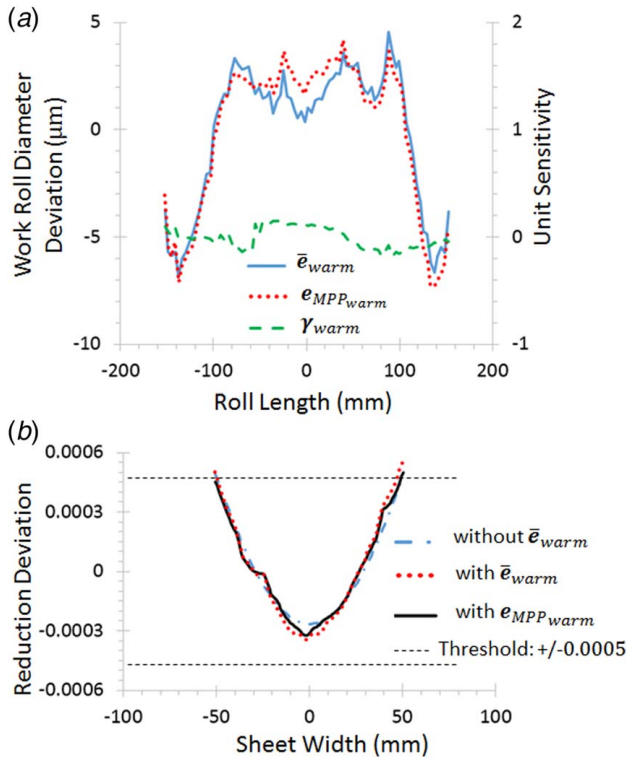

Fig. 7 Comparison of results for "warm" roll considering the random field based on measured work-roll diameter deviations: (*a*) mean measured diameter deviation for the warm roll ($\bar{e}_{warm}$), most probable point (MPP) of failure values on the warm roll with correlated random variables ($e_{MPP_{warm}}$), and unit sensitivity (right axis) of the reliability to each random variable on the warm roll with correlated variables (γ_{warm}) and (*b*) corresponding sheet reduction deviation profiles for mean measured diameter deviation, as well as independent and correlated MPP diameter deviations values on warm roll

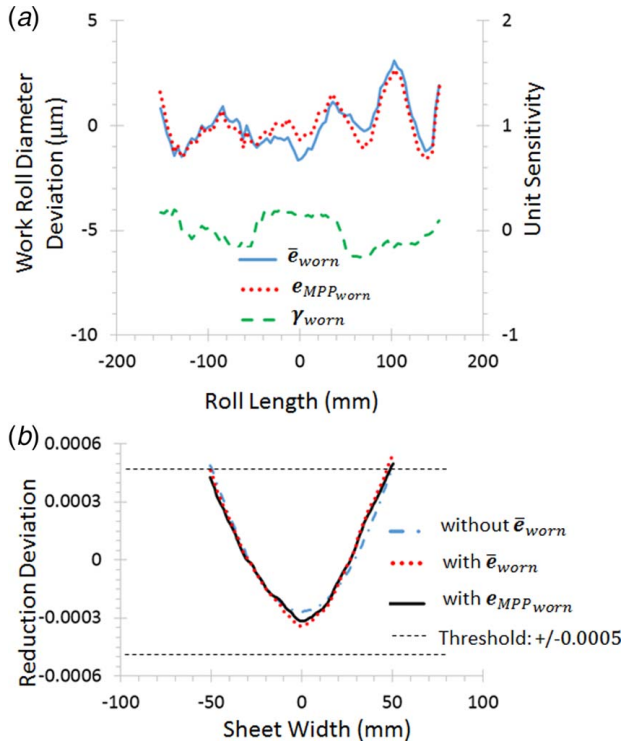

Fig. 8 Comparison of results for "worn" roll considering the random field based on measured work-roll diameter deviations: (*a*) mean measured diameter deviation for the worn roll ($\bar{e}_{worn}$), most probable point (MPP) of failure values on the worn roll with correlated random variables ($e_{MPP_{worn}}$), and unit sensitivity (right axis) of the reliability to each random variable on the worn roll with correlated variables (γ_{worn}) and (*b*) corresponding sheet reduction deviation profiles for mean measured diameter deviation, as well as independent and correlated MPP diameter deviations values on worn roll

defects are most likely to occur when the work-roll is warm. In addition, based on the reliabilities in Table 2, using a worn work-roll for the next rolling pass is more likely to produce sheet flatness defects than when installing a newly ground roll.

Similar to Fig. 6 for the new work-roll, Figs. 7 and 8 show the MPP and unit sensitivity of the work-roll diameter deviations for both warm and worn working conditions. The SSM-FEM model shows that the diameter deviations should be reduced at about 25 mm from the strip edge and that corresponding reduction deviations should decrease at +50.8 mm in both $\boldsymbol{e}_{MPP_{warm}}$ and $\boldsymbol{e}_{MPP_{worn}}$. Overall, the warm work-roll is revealed to be less sensitive in comparison to both the new and worn rolls; the reason is that larger statistical variance and stronger correlation (see Fig. 2) can reduce the sensitivity, as indicated by Eqs. (14)–(16). In other words, changing the work-roll diameter profile to correct for sheet flatness defects proves less effective when the roll is warm. From a practical viewpoint, insights gleaned from this changing unit sensitivity for the warm roll can provide an improved understanding of the performance of spray header (nozzle-based) roll cooling systems as discussed in Introduction section.

Finally, it is notable that the general wedge-shaped reduction deviations are maintained in all MPPs in Figs. 6–8. This low-order variation would be modified through the use of any conventional low-fidelity flatness control mechanism (e.g., work-roll bending or additional roll crowns). Accordingly, the incorporation of this stochastic roll-stack model prediction with the use of conventional control mechanisms can augment flatness control capability to address both low-fidelity (natural roll-stack deformation) and high-fidelity (roll diameter deviation)-induced sheet flatness issues and requirements. In practice, the new SSM-FEM could be incorporated into an optimization method to create a reliability-based optimum roll-stack model, the aim of which could be to design high-fidelity work-roll diameter profiles in the presence of the random field diameter deviations.

Conclusion

SSM-FEM is demonstrated to compute 3D roll-stack deformation and contact mechanics behaviors for a thin-sheet, 4-high rolling mill in the presence of work-roll diameter random field deviations. The new, stochastic roll-stack model integrates the simplified-mixed finite element method with an analytical, safety index-based first-order reliability method. Work-roll diameter deviations are modeled as random fields, and the SSM-FEM allows for mathematically rigorous stochastic analysis of the effects of correlated roll diameter deviations (obtained by measurements) on the resulting strip thickness profile and flatness. The results of this study bring the following major conclusions:

- A deterministic (nonrandom variable capable) roll-stack model cannot provide sufficiently accurate prediction in sheet flatness quality since such models do not consider random variations of the work-roll diameter profile (among other uncertainties).
- It is an improper assumption that work-roll diameter deviations along the roll length are independent of one another; spatial correlation among the random variables (i.e., presence of a random field) influences the sheet flatness reliability and its sensitivity profile to the work-roll diameter deviations.
- The consideration of work-roll diameter as a random field means that the model identifies corrections based on all (correlated) work-roll diameter deviations, rather than only the local problematic ones, as is the case with the independent random variables assumption.
- Unit sensitivity of the work-roll diameter deviations provides for a stochastic understanding of the connection between the roll grinding process and the cold rolling process; the grinding precision cannot be relaxed even if the location of a significant work-roll deviation is external to the roll/sheet contact region. This is because of the strong statistical correlation among spatially separated roll diameter deviations.
- Both thermal expansion and wear of the work-rolls is shown to decrease the sheet flatness reliability compared to the newly machined (ground) work-rolls because of the changes they create in the statistical correlations between roll diameter deviations.
- Roll thermal expansion amplifies both means and variances of the roll diameter deviations and also induces additional correlation in the residual grinding error, reducing sheet flatness reliability. The sensitivity of the reliability to diameter deviations is also less for the warm roll than for new and worn rolls, which means that the work-roll is more likely to produce flatness defects after some period of heating by friction/plastic dissipation during rolling; the warm condition is also that in which target flatness quality is least likely to be recovered.

Acknowledgment

The authors gratefully acknowledge support for this work from the National Science Foundation (Grant No. CMMI-1555531).

Conflict of Interest

There are no conflicts of interest.

Data Availability Statement

The datasets generated and supporting the findings of this article are obtainable from the corresponding author upon reasonable request. The authors attest that all data for this study are included in the paper.

References

[1] Malik, A. S., and Grandhi, R. V., 2008, "A Computational Method to Predict Strip Profile in Rolling Mills," J. Mater. Process. Technol., **206**(1–3), pp. 263–274.
[2] Zhang, F., Malik, A. S., and Yu, H., 2018, "High-Fidelity Roll Profile Contact Modeling by Simplified Mixed Finite Element Method," ASME 2018 13th International Manufacturing Science and Engineering Conference. Volume 4: Processes, College Station, TX, June 18–22, ASME, p. V004T03A034.
[3] Ahmed, R., and Sutcliffe, M., 2001, "An Experimental Investigation of Surface Pit Evolution During Cold-Rolling or Drawing of Stainless Steel Strip," ASME J. Tribol., **123**(1), pp. 1–7.
[4] Sutcliffe, M. P., 2002, "Surface Finish and Friction in Cold Metal Rolling," *Metal Forming Science and Practice*, J. G. Lenard, ed., Elsevier, UK.
[5] Siddhpura, M., and Paurobally, R., 2012, "A Review of Chatter Vibration Research in Turning," Int. J. Mach. Tools Manuf., **61**, pp. 27–47.
[6] Zhang, F., and Malik, A. S., 2021, "An Efficient Multi-Scale Modeling Method That Reveals Coupled Effects Between Surface Roughness and Roll-Stack Deformation in Cold Sheet Rolling," ASME J. Manuf. Sci. Eng., **143**(10), p. 101005.
[7] Linghu, K., Jiang, Z., Zhao, J., Li, F., Wei, D., Xu, J., Zhang, X., and Zhao, X., 2014, "3D FEM Analysis of Strip Shape During Multi-Pass Rolling in a 6-High CVC Cold Rolling Mill," Int. J. Adv. Manuf. Technol., **74**(9–12), pp. 1733–1745.
[8] Hou, Z. B., and Komanduri, R., 2003, "On the Mechanics of the Grinding Process—Part I. Stochastic Nature of the Grinding Process," Int. J. Mach. Tools Manuf., **43**(15), pp. 1579–1593.
[9] Peklenik, J., 1964, "Contribution to the Theory of Surface Characterization," CIRP Ann., **12**, pp. 173–178.
[10] Peklenik, J., 1967, "Investigation of the Surface Typology," CIRP Ann., **15**, p. 381.
[11] Nguyen, T., and Butler, D., 2005, "Simulation of Precision Grinding Process, Part 1: Generation of the Grinding Wheel Surface," Int. J. Mach. Tools Manuf., **45**(11), pp. 1321–1328.
[12] Cao, Y., Guan, J., Li, B., Chen, X., Yang, J., and Gan, C., 2013, "Modeling and Simulation of Grinding Surface Topography Considering Wheel Vibration," Int. J. Adv. Manuf. Technol., **66**(5–8), pp. 937–945.
[13] Downey, G., 1996, "Differential Roll Cooling to Control Strip Flatness and Shape," Steel Times, **224**(6), p. 226.
[14] Lenard, J. G., 2014, *Primer on Flat Rolling*, 2nd ed., Elsevier, Amsterdam.
[15] Ginzburg, V. B., 1993, *High-Quality Steel Rolling: Theory and Practice*, CRC Press, Boca Raton, FL.
[16] Zhang, F., and Malik, A., 2018, "A Roll-Stack Contact Mechanics Model to Predict Strip Profile in Rolling Mills With Asymmetric, Continuously Variable Crown Rolls," ASME J. Manuf. Sci. Eng., **140**(1), p. 011008.
[17] Haldar, A., and Mahadevan, S., 2000, *Reliability Assessment Using Stochastic Finite Element Analysis*, John Wiley & Sons, New York.

[18] Nikolaidis, E., Ghiocel, D. M., and Singhal, S., 2004, *Engineering Design Reliability Handbook*, CRC Press, Boca Raton, FL.
[19] Malik, A. S., and Hinton, J. L., 2012, "Displacement of Multiple, Coupled Timoshenko Beams in Discontinuous Nonlinear Elastic Contact, With Application to Rolling Mills," ASME J. Manuf. Sci. Eng., **134**(5), p. 051009.
[20] Guo, R.-M., 1997, "Prediction of Strip Profile in Rolling Process Using Influence Coefficients and Boussinesq's Equations," ASME J. Manuf. Sci. Eng., **119**(2), pp. 220–226.
[21] Vanmarcke, E., and Grigoriu, M., 1983, "Stochastic Finite Element Analysis of Simple Beams," J. Eng. Mech., **109**(5), pp. 1203–1214.
[22] Shinozuka, M., and Deodatis, G., 1991, "Simulation of Stochastic Processes by Spectral Representation," ASME Appl. Mech. Rev., **44**(4), pp. 191–204.
[23] Segerlind, L. J., 1987, *Applied Finite Element Analysis*, 2nd ed., John Wiley & Sons, New York.
[24] Hasofer, A. M., and Lind, N. C., 1974, "Exact and Invariant Second-Moment Code Format," J. Eng. Mech. div., **100**(1), pp. 111–121.
[25] Rackwitz, R., and Fiessler, B., 1976, *Note on Discrete Safety Checking When Using Non-Normal Stochastic Models for Basic Variables. Loads Project Working Session*, Massachusetts Institute of Technology, Cambridge, MA.
[26] Chen, X., and Lind, N., 1982, "Fast Probability Integration by Three-Parameter Normal Tail Approximation," Struct. Saf., **1**(4), pp. 269–276.
[27] Wu, Y.-T., and Wirsching, P. H., 1987, "New Algorithm for Structural Reliability Estimation," J. Eng. Mech., **113**(9), pp. 1319–1336.
[28] Bazoune, A., Khulief, Y. A., and Stephen, N.G., 2003, "Shape Functions of Three-Dimensional Timoshenko Beam Element," J. Sound Vib., **259**(2), pp. 473–480.
[29] Malik, A. S., 2007, "Rolling Mill Optimization Using an Accurate and Rapid New Model Mill Deflection and Strip Thickness Profile," Ph.D. thesis, Wright State University, Dayton, OH.
[30] Matsubara, S., Hara, K., and Takezoe, A., 1989, "Optimization of Work Roll Taper for Extremely-Thin Strip Rolling," ISIJ Int., **29**(1), pp. 58–63.